DTIC
SELECTED
SEP 0 5 1995
F

CRREL

A Physically Based Model of the Form Drag Associated with Sastrugi

Edgar L Andreas

July 1995

19950901 082

Abstract

On Ice Station Weddell, some characteristics of the neutral-stability air–ice drag coefficient at a reference height of 10 m (C_{DN10}) were observed that had not been documented before. The main finding was that wind-driven snow continually alters the sea ice surface; the resulting snowdrifts determine how large C_{DN10} is. In particular, this report describes three observations and attempts to explain them: 1) C_{DN10} is near 1.5×10^{-3} when the wind is well aligned with the drifted snow; 2) C_{DN10} is near 2.5×10^{-3} when the wind makes a large angle with the dominant orientation of the snowdrifts; 3) C_{DN10} can increase by 20% if, after being well aligned with the drift patterns, the mean wind direction shifts by as little as 20°. To investigate this behavior of C_{DN10}, this report adapts a model developed by Raupach that partitions the total surface stress into contributions from form drag and skin friction. With reasonable choices for free model parameters and with little fine-tuning, this physically based model can reproduce the three main observations. In other words, the model seems to include the basic physics of air–ice momentum exchange. This modeling implies that 10-cm-high sastrugi-like roughness elements, rather than pressure ridges, sustain most of the form drag over compact sea ice in the western Weddell Sea. Lastly, the report speculates on what the observations and this model say about how to parameterize C_{DN10} over snow-covered sea ice.

Cover: Drifting snow on Ice Station Weddell. Photograph by Keran Claffey.

CRREL Report 95-16

**US Army Corps
of Engineers**

Cold Regions Research &
Engineering Laboratory

A Physically Based Model of the Form Drag Associated with Sastrugi

Edgar L Andreas

July 1995

Accesion For		
NTIS CRA&I	☑	
DTIC TAB	☐	
Unannounced	☐	
Justification		
By		
Distribution /		
Availability Codes		
Dist	Avail and / or Special	
A-1		

DTIC QUALITY INSPECTED 5

PREFACE

Dr. Edgar L Andreas, Physicist, Snow and Ice Division, Research and Engineering Directorate, U.S. Army Cold Regions Research and Engineering Laboratory, prepared this report. He thanks Keran J. Claffey, who played a large role in collecting the data on Ice Station Weddell, and R.B. Haehnel and Dr. S.C. Colbeck, who reviewed the manuscript.

CONTENTS

ILLUSTRATIONS

A Physically Based Model of the Form Drag Associated with Sastrugi

EDGAR L ANDREAS

INTRODUCTION

The neutral-stability, 10-m air–ice drag coefficients (C_{DN10}) reported by Andreas and Claffey (1995; henceforth, AC95) clearly depend on how wind-driven snow alters the sea ice surface. Figure 1 shows the time series of Ice Station Weddell (ISW) C_{DN10} values and hourly averages of the wind speed and direction measured at 5 m. These C_{DN10} values range between 1.27×10^{-3} and 2.54×10^{-3} but are not randomly scattered between these limits. Rather, they generally cluster or depend coherently on time. For example, in AC95 we focused on the events on Julian days 64 and 65 and 79 and 80. In Figure 1, we see that, on these days, the 5-m wind speed was typically 8 m/s or higher, the wind direction was fairly constant, and C_{DN10} decreased consistently with time.

Our explanation for this sequence was that winds of 6–8 m/s, and higher, redistribute the mobile snow: snowdrifts perpendicular to the wind erode; and the new drifts, built parallel with the mean wind, streamline the surface. Consequently, if these eroding winds persist and their direction remains relatively constant for just 12 hours, C_{DN10} will decrease by as much as 30%. If, after establishing a drift pattern, however, the wind shifts by as little as 20°, it will face a rougher surface, and measured C_{DN10} values will increase.

There are several other events in Figure 1 that demonstrate this same smoothing in the presence of a moderate, directionally constant wind (for example, see days 86 and 87). Thus, the sequence is repeatable and, in fact, seems to be the key to understanding air–ice momentum exchange in the western Weddell Sea—and probably over most other sea ice regions as well.

Form drag sustained by the snowdrifts must explain the behavior of the C_{DN10} values that we observed. Others have also recognized that form
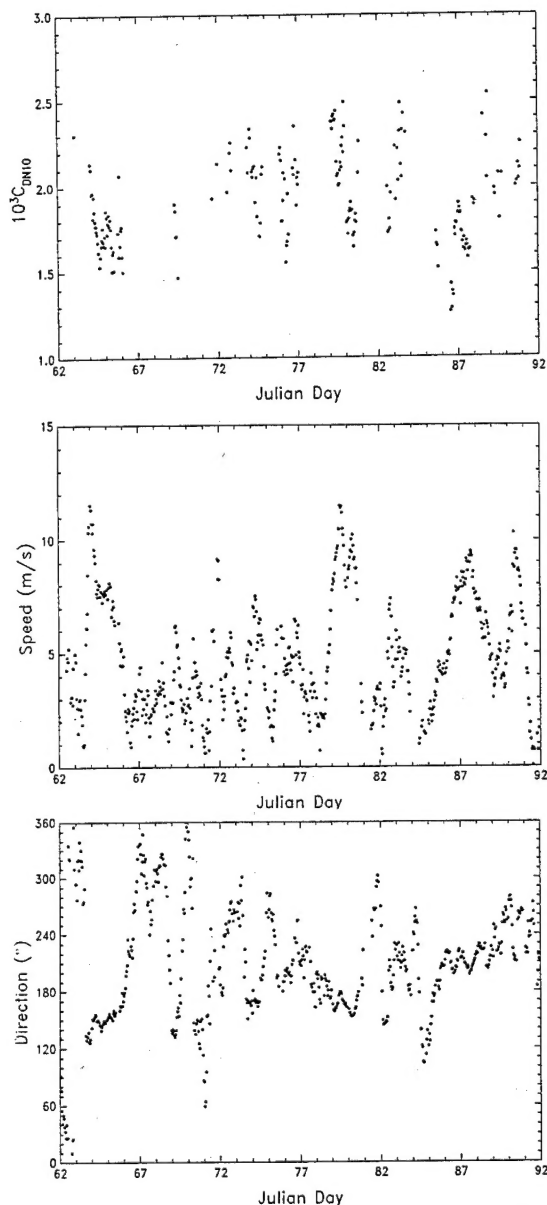

Figure 1. Time series of the Ice Station Weddell (ISW) C_{DN10} values reported in Andreas and Claffey (1995) and hourly averages of the wind speed and direction at 5 m.

drag can, at times, be an important means for transferring momentum to a surface. For example, Lettau (1969) offered a heuristic formula involving obstacle geometry and silhouette area to parameterize the roughness lengths that Kutzbach (1961) measured during his famous bushel basket experiment on Lake Mendota. Arya (1973, 1975) assumed that pressure ridges were the roughness elements responsible for most of the form drag over Arctic sea ice and developed a model to partition the total stress into skin friction and form drag on the basis of ridging intensity. Banke et al. (1976, 1980) investigated the pressure distribution around Arctic pressure ridges 1–3 m high in an attempt to determine the form drag coefficient for these. But their ultimate parameterization for C_{DN10} (also Banke and Smith 1973) is more in line with our findings; they showed that

$$10^3 \, C_{DN10} = 1.10 + 0.072 \, \xi \qquad (1)$$

where ξ (in centimeters) is the root-mean-square surface roughness for roughness elements with wavelengths shorter than 13 m. That is, the smaller scale roughness dominates the momentum exchange. Jackson and Carroll (1978) reached the same conclusion. They showed that the angle between the mean wind and the dominant axis of the sastrugi at the South Pole determined the roughness length; they then developed a model based on Lettau's to explain this effect.

More recently, Raupach (1992; henceforth, R92; also Raupach et al. 1993) developed a more sophisticated model, based on dimensional analysis and two physically reasonable hypotheses, to partition the total surface stress into contributions from form drag and from the stress on the underlying surface. That model is the basis of the analysis here. I adapt Raupach's model to evaluate the stress partitioning for a field of sastrugi-like snowdrifts. That model predicts the drag coefficient evaluated at the top of the roughness elements; I show how this quantity is related to C_{DN10}, which, in turn, is monotonically related to the roughness length z_0 through

$$C_{DN10} = k^2 \, \{\ln[(10 - d)/z_0]\}^{-2} . \qquad (2)$$

Here, k ($= 0.4$) is the von Kármán constant, and z_0 and the displacement height d must be in meters.

My objective is to see whether, with reasonable choices for snowdrift geometry and other

free model parameters, R92's model can account for the behavior of C_{DN10} at ISW that we documented in AC95. In particular, the three main observations that I hope to explain are as follows:

1. C_{DN10} is near 1.5×10^{-3} when the wind is aligned with a well-developed field of drifted snow.

2. C_{DN10} is near 2.5×10^{-3} when the mean wind direction makes a large angle (say 50–140°) with the dominant axis of the drifts.

3. C_{DN10} can increase by roughly 20% if, after being aligned with a developed (or developing) field of drifted snow, the wind turns by as little as 20°.

RAUPACH'S MODEL ADAPTED TO DRIFTED SNOW

Geometry

Because during our deployment on ISW the wind was directionally quite variable, the surface never developed the deep, elaborate fields of sastrugi that Mellor (1965) and Jackson and Carroll (1978) observed on the Antarctic continent. Rather, on ISW, the drifts were sparsely distributed and rudimentary. When the wind reached 6–8 m/s, linear sastrugi-like drifts would begin forming behind any protruding obstacles. The drifts would grow as the wind persisted; but when the wind direction changed, these drifts would erode in winds above the 6- to 8-m/s threshold. Thus, the drifts that determined the surface roughness on ISW were generally small. The scour marks that Allen (1965) described and named scour-remnant ridges may well be precursors to these rudimentary sastrugi.

Figure 2 shows a typical leveling profile of the snow and sea ice surfaces in the vicinity of the profiling mast described in AC95. We made seven such leveling surveys during our deployment on ISW. The profiles show that snow tends to collect around obstacles in the underlying ice. The root-mean-square (rms) roughness of the snow surface in this particular profile is 11 cm; its ice-surface roughness is 9 cm. In the seven surface profiles that we collected, the rms snow-surface roughness ranged from 9 to 26 cm; the ice-surface roughness ranged from 9 to 28 cm. A value in this range is a reasonable choice for the nominal height of the snow-surface roughness elements.

Figure 3 shows the idealized geometry of the roughness elements that I will treat with R92's model. These are rudimentary sastrugi with
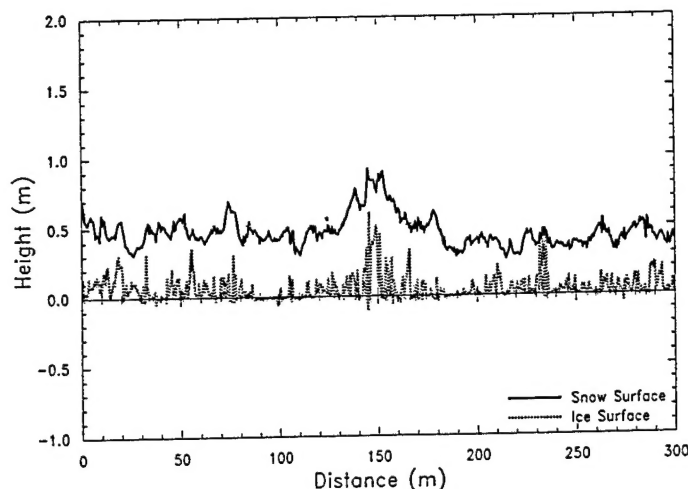
Figure 2. Snow and ice surface elevations near our ISW profile tower on Julian day 78 (in 1992). The sampling interval was 0.5 m. The profiling line is not necessarily aligned with the mean wind.
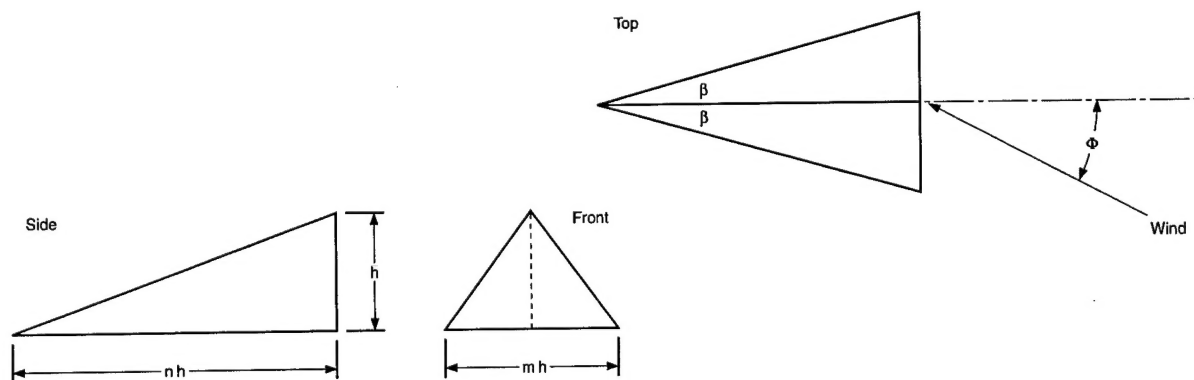

Figure 3. Geometry of the sastrugi-like snowdrifts being modeled here.

height h, width mh, and length nh. The angle Φ describes how the mean wind is oriented with respect to the sastrugi. When the wind has been blowing with constant direction at speeds of 6–8 m/s, or higher, for several hours, Φ will be zero.

From the discussion in the penultimate paragraph, we see that h is 5–20 cm. Descriptions of drifted snow in the literature (Finney 1939, Mellor 1965, Jackson and Carroll 1978) and Plate's (1971, Figure 4.17) pressure distribution around roughness elements similar to that in Figure 3 suggest that n is about 10. From Mellor's (1965) description of sastrugi, I assume that m is about 4. Notice, these parameters imply that, in Figure 3

$$\beta = \arctan(m/2n) = 11.3°. \tag{3}$$

One of the key parameters in R92's model is λ, the frontal area of a typical roughness element

per unit ground area. Suppose the fraction of the area covered by the sastrugi-like roughness elements is γ. Thus, from Figure 3, the unit area represented by each roughness element is $mnh^2/2\gamma$. The base length of the triangular frontal area that each roughness element presents to the wind, $L(\Phi)$, is a function of Φ. Likewise, the silhouette area presented, $A(\Phi)$, is simply

$$A(\Phi) = \frac{1}{2}hL(\Phi). \tag{4}$$

Consequently, λ is also a function of Φ

$$\lambda(\Phi) = \frac{2\gamma A(\Phi)}{mnh^2} = \frac{\gamma L(\Phi)}{mnh}. \tag{5}$$

In Figure 3, we see that there are four Φ regions for which a roughness element presents different faces to the wind for $0 \leq \Phi \leq 180°$ (symmetric for $0 \geq \Phi \geq -180°$). These and the associated values of L, A and λ follow.

3

Region I: $0° \le \Phi \le \beta$

Here the wind sees only the front triangular face. Thus

$$L(\Phi) = mh \cos\Phi \qquad (6a)$$

$$A(\Phi) = (mh^2/2) \cos\Phi \qquad (6b)$$

$$\lambda(\Phi) = (\gamma/n) \cos\Phi . \qquad (6c)$$

Region II: $\beta \le \Phi \le 90°$

Here the wind sees both the front triangular face and the side ridge. Thus

$$L(\Phi) = nh \sin\Phi + (mh/2) \cos\Phi \qquad (7a)$$

$$A(\Phi) = (h^2/2)[n \sin\Phi + (m/2) \cos\Phi] \qquad (7b)$$

$$\lambda(\Phi) = \gamma[m^{-1} \sin\Phi + (2n)^{-1} \cos\Phi] . \qquad (7c)$$

Region III: $90° \le \Phi \le 180° - \beta$

Here the wind sees only the side ridge. Thus

$$L(\Phi) = nh \sin\Phi - (mh/2) \cos\Phi \qquad (8a)$$

$$A(\Phi) = (h^2/2) [n \sin\Phi - (m/2) \cos\Phi] \qquad (8b)$$

$$\lambda(\Phi) = \gamma[m^{-1} \sin\Phi - (2n)^{-1} \cos\Phi] . \qquad (8c)$$

Region IV: $180° - \beta \le \Phi \le 180°$

Here the flow sees both side ridges as it approaches from the rear of the drift. Thus

$$L(\Phi) = -mh \cos\Phi \qquad (9a)$$

$$A(\Phi) = -(mh^2/2) \cos\Phi \qquad (9b)$$

$$\lambda(\Phi) = -(\gamma/n) \cos\Phi . \qquad (9c)$$

Partitioning the stress

R92's intent was to partition the total surface stress (τ) into contributions from form drag (τ_R) and from stress on the underlying surface (the skin friction, τ_S). In general

$$\tau = \tau_R + \tau_S . \qquad (10)$$

There is another potential sink for the momentum in eq 10 that R92 did not treat. Over erodible surfaces, saltating particles may extract momentum from the air because of their inertia. Neither τ_R nor τ_S reflects this momentum exchange. That saltation layer, however, is quite thin—on the order of a centimeter (Owen 1964, Radok 1968,

AC95). Thus, since R92 models eq 10 for heights of order h and higher—well above the saltation layer—eq 10 need not include a term to account for particle inertia. Above the saltation layer, the concentration of blowing and drifting snow is too low to affect the dynamics of the flow.

R92 modeled the stress on the underlying surface as

$$\tau_S(\lambda) = \rho C_{Sh} U_h^2 \exp\left[-c_1 \lambda(\Phi) \frac{U_h}{u_*}\right] . \qquad (11)$$

Here, C_{Sh} is the drag coefficient of the underlying surface referenced to a height h, which is where the wind speed U_h is evaluated. Also in eq 11, ρ is the air density; u_*, the friction velocity, $u_* = (\tau/\rho)^{1/2}$; and c_1, an empirical constant. The exponential term in eq 11 accounts for the sheltering of the underlying surface by the roughness elements. That is, when the roughness elements are small or sparse and $\lambda(\Phi)$, thus, is small, eq 11 reduces to $\tau_S = \rho C_{Sh} U_h^2$, the usual expression for the skin friction over a smooth surface. On the other hand, when the roughness elements have a large frontal area or are densely packed, $\lambda(\Phi)$ is large, and τ_S approaches zero. In this case, the roughness elements completely shelter the surface; thus, skin friction can provide none of the stress.

We can infer the value of C_{Sh} appropriate for smooth, snow-covered surfaces from Overland's (1985) review and from the measurements reported by Banke et al. (1980) and Kondo and Yamazawa (1986). The lowest value for C_{DN10} reported by Overland and Kondo and Yamazawa is roughly 1.1×10^{-3}. Coincidentally, Figure 4 in Banke et al. implies that the value of C_{DN10} for completely smooth sea ice is 1.10×10^{-3}. Call this minimum skin friction coefficient C_{S10}.

Converting C_{S10} to C_{Sh}, however, is not straightforward: We do not know the displacement height d a priori; and near the tops of the roughness elements, the semi-logarithmic profile law (see eq 2) is not accurate. I will explain how I deal with these complications later; here, suffice it to say, I obtain C_{Sh} from C_{S10}.

R92 wrote a general expression for the force caused by form drag on an isolated roughness element as

$$F_D = \rho C_R A U_h^2 \qquad (12)$$

where C_R is the drag coefficient of the obstacle, and A is its silhouette area. Here, I must modify

Raupach's model, however. In my model, the obstacle's aerodynamic properties likely change as its orientation with the wind changes. Otherwise, the concept of streamlining would be meaningless. Thus, C_R and A must depend on Φ. But because I could find no study in the literature that reported the aerodynamic properties of an obstacle like that depicted in Figure 3, I assume that the drag contributions from the various faces are additive. Mathematically, my hypothesis is

$$F_D(\Phi) = \rho U_h^2 \sum_i C_{Ri}(\Phi) A_i(\Phi) \qquad (13)$$

where C_{Ri} is the drag coefficient for a particular face of the sastrugi-like obstacle, and A_i is the silhouette area of that face. The sum is over all faces presented to the wind at angle Φ.

The obstacle in Figure 3 presents only three faces. When $0° \leq \Phi \leq 90°$, the wind can see the front triangular face; this has form drag coefficient C_{R1}. When $\beta \leq \Phi \leq 180° - \beta$, the wind can see the side ridge; this has drag coefficient C_{R2}. When $180° - \beta \leq \Phi \leq 180°$, the wind can see only the rear silhouette; this has drag coefficient C_{R3}.

As I mentioned, I found no study that evaluated C_R for the obstacle geometry I use here. But on reviewing several studies that treated somewhat similar geometries (i.e., Arie and Rouse 1956; Arya 1973, 1975; Banke et al. 1976, 1980; Taylor 1988), I estimated what I feel are representative values for the three faces. Here, I use $C_{R1} = 0.10$, $C_{R2} = 0.30$, and $C_{R3} = 0.30$.

Continuing now with R92's model, if p roughness elements cover a ground area S, the stress they produce through form drag is

$$\tau_R(\Phi, p) = \frac{p}{S}\left[\rho U_h^2 \sum_i C_{Ri}(\Phi) A_i(\Phi)\right]\left(1 - \frac{V}{Sh}\right)^p. \quad (14)$$

Here, V is the volume sheltered by an individual roughness element; the term raised to power p, thus, represents a mutual sheltering effect.

In my model, from eq 5

$$\frac{p}{S} = \frac{2\gamma}{mnh^2} = \frac{\lambda(\Phi)}{A(\Phi)}. \qquad (15)$$

Using this in eq 14 gives

$$\tau_R(\Phi, p) = \frac{\lambda(\Phi)}{A(\Phi)}\left[\rho U_h^2 \sum_i C_{Ri}(\Phi) A_i(\Phi)\right]$$

$$\cdot \left(1 - \frac{\lambda(\Phi)V}{phA(\Phi)}\right)^p. \qquad (16)$$

In the limit of large p

$$\left(1 - \frac{\lambda(\Phi)V}{phA(\Phi)}\right)^p \approx \exp\left[\frac{-\lambda(\Phi)V}{hA(\Phi)}\right]. \qquad (17)$$

Finally, following R92, for m and n greater than 1, I estimate the sheltered volume to be

$$V = \frac{1}{2}c_2 L(\Phi)h^2 \frac{U_h}{u_*} \qquad (18)$$

where c_2 is another empirical constant. Hence, using eq 5, 17 and 18 in eq 16, we get

$$\tau_R(\Phi) = \lambda(\Phi)\left[\rho U_h^2 \sum_i C_{Ri}(\Phi)\frac{A_i(\Phi)}{A(\Phi)}\right]$$

$$\cdot \exp\left[-c_2 \lambda(\Phi)\frac{U_h}{u_*}\right]. \qquad (19)$$

In eq 19, define

$$\hat{C}_R(\Phi) \equiv \sum_i C_{Ri}(\Phi)\frac{A_i(\Phi)}{A(\Phi)}. \qquad (20)$$

For the four Φ regions identified earlier, $\hat{C}_R$ follows.

Region I: $0° \leq \Phi \leq \beta$

$$\hat{C}_{RI} = C_{R1}. \qquad (21a)$$

Region II: $\beta \leq \Phi \leq 90°$

$$\hat{C}_{RII} = \frac{C_{R1}m\cos\Phi + C_{R2}[n\sin\Phi - (m/2)\cos\Phi]}{n\sin\Phi + (m/2)\cos\Phi}. \qquad (21b)$$

Region III: $90° \leq \Phi \leq 180° - \beta$

$$\hat{C}_{RIII} = C_{R2}. \qquad (21c)$$

Region IV: $180° - \beta \leq \Phi \leq 180°$

$$\hat{C}_{RIV} = C_{R3}. \qquad (21d)$$

Combining eq 11, 19 and 20 in eq 10, we get

$$\tau(\Phi) = \rho U_h^2\left\{C_{Sh}\exp\left[-c_1\lambda(\Phi)\frac{U_h}{u_*}\right]\right.$$

$$\left. +\lambda(\Phi)\hat{C}_R(\Phi)\exp\left[-c_2\lambda(\Phi)\frac{U_h}{u_*}\right]\right\}. \qquad (22)$$

5

To make solving eq 22 easier, R92 assumed that $c_1 = c_2 = c$; for c he used 0.25, which provided the best fit to the data that he tested his model against. With this assumption, eq 22 reduces to

$$\tau(\Phi) = \rho U_h^2 \left[C_{Sh} + \lambda(\Phi)\hat{C}_R(\Phi) \right] \exp\left[-c\lambda(\Phi)\frac{U_h}{u_*} \right]. \quad (23)$$

Notice

$$\frac{\tau(\Phi)}{\rho U_h^2} = \frac{u_*^2}{U_h^2} \equiv C_{Dh} \equiv \frac{1}{r^2} \quad (24)$$

is the drag coefficient for the total surface stress referenced to height h. On inserting this definition and rearranging terms in eq 23, we get

$$\frac{c\lambda(\Phi)r}{2} \exp\left[\frac{-c\lambda(\Phi)r}{2} \right]$$
$$= \frac{c\lambda(\Phi)}{2} \left[C_{Sh} + \lambda(\Phi)\hat{C}_R(\Phi) \right]^{-1/2}. \quad (25)$$

This has the form

$$X e^{-X} = a \quad (26)$$

where a is a constant for a given value of Φ.

I solved eq 26 for X using Newton's method; the solution required only two to three iterations. There are multiple solutions to eq 26, however; we must select the right one. As R92 explained, eq 26 has the following properties:

For $0 < a < e^{-1}$, eq 26 has two solutions, X_1 and X_2, where $X_1 < 1$ and $X_2 > 1$.

For $a = e^{-1}$, $X = 1$.

For $a > e^{-1}$, there is no solution to eq 26. The only nontrivial case is the first of these; and X_1 is the only physical solution, since X must approach zero as either $\lambda(\Phi)$ or a approaches zero. Thus, to start Newton's method, my first guess was $X = a$.

Solving eq 26 yields X, which, in turn, is related to the total drag coefficient we seek

$$C_{Dh}^{-1/2} = \frac{2X}{c\lambda(\Phi)}. \quad (27)$$

Notice, to check this solution, we can make an asymptotic approximation in eq 23. When $\lambda(\Phi)$ is near zero

$$C_{Dh} = C_{Sh} + \lambda(\Phi)\hat{C}_R(\Phi). \quad (28)$$

Displacement height

To convert the total drag coefficient C_{Dh} to its 10-m value, we need to know the wind speed profile law. When a surface is covered with roughness elements that are much larger than z_0, it is often necessary to include a displacement height d (Thom 1971) in the semi-logarithmic wind profile. That is

$$\frac{U(z)}{u_*} = \frac{1}{k} \ln\left(\frac{z-d}{z_0} \right) \quad (29)$$

where $U(z)$ is the average wind speed at height z.

But near the tops of the roughness elements, eq 29 cannot be accurate because of the enhanced turbulence there created by flow around these obstacles. R92 therefore hypothesized that, for $h \leq z \leq z_w$

$$\frac{U(z)}{u_*} = \frac{1}{k}\left[\ln\left(\frac{z-d}{z_0} \right) + \psi\left(\frac{z-d}{z_w-d} \right) \right] \quad (30)$$

where ψ is a profile influence function similar to the stability corrections required by Monin-Obukhov similarity. At z_w and above, ψ is zero.

R92 went on to show that

$$\psi\left(\frac{z-d}{z_w-d} \right) = \frac{z-z_w}{z_w-d} + \ln\left(\frac{z_w-d}{z-d} \right) \quad (31)$$

and that

$$z_w - d = c_w(h-d) \quad (32)$$

where c_w is a constant. He also defined

$$\Psi_h \equiv \psi\left(\frac{h-d}{z_w-d} \right) = \ln(c_w) + c_w^{-1} - 1 \quad (33)$$

which will be useful shortly. Notice, there are errors in two of R92's equations (eq 29 and 31). In an unpublished correction to his paper dated 23 October 1992, Raupach explained that, in light of these errors, c_w is approximately 4 rather than 1.5, the value he originally gave. Hence, $\psi_h = 0.64$, a value independent of surface properties.

Equation 32 implies that

$$z_w = c_w h + (1 - c_w)d. \quad (34)$$

With $c_w = 4$ and the assumption that $z_w > h$, eq 34 implies that $d < h$: The displacement height is always less than the height of the roughness elements.

To obtain C_{DN10} from C_{Dh}, we must match the profile laws, eq 29 and 30, at z_w. From eq 29 and 32, we have the following results for $z \geq z_w$

$$C_{DN10}^{-1/2} \equiv \frac{U(10)}{u_*} = \frac{1}{k}\ln\left(\frac{10-d}{z_0}\right) \qquad (35)$$

and

$$C_{Dz_w}^{-1/2} \equiv \frac{U(z_w)}{u_*} = \frac{1}{k}\left[\ln\left(\frac{h-d}{z_0}\right)+\ln(c_w)\right] \quad (36)$$

where h, d, z_0 and z_w must be in meters. Subtracting eq 35 from 36, we get

$$C_{Dz_w}^{-1/2} = C_{DN10}^{-1/2} + \frac{1}{k}\left[\ln\left(\frac{h-d}{10-d}\right)+\ln(c_w)\right]. \quad (37)$$

From eq 30–33, for $h \leq z \leq z_w$

$$C_{Dh}^{-1/2} \equiv \frac{U_h}{u_*} = \frac{1}{k}\left[\ln\left(\frac{h-d}{z_0}\right)+\psi_h\right] \qquad (38)$$

and

$$C_{Dz_w}^{-1/2} = \frac{U(z_w)}{u_*} = \frac{1}{k}\left[\ln\left(\frac{h-d}{z_0}\right)+\ln(c_w)\right]. \quad (39)$$

Subtracting eq 38 from 39 yields

$$C_{Dz_w}^{-1/2} = C_{Dh}^{-1/2} + \frac{1}{k}\left[\ln(c_w)-\psi_h\right]. \qquad (40)$$

On equating eq 37 and 40, we finally can relate C_{DN10} to C_{Dh}

$$C_{DN10}^{-1/2} = C_{Dh}^{-1/2} + \frac{1}{k}\left[\ln\left(\frac{10-d}{h-d}\right)-\psi_h\right]. \qquad (41)$$

We still do not know the displacement height d, however.

Thom (1971) identified d as the effective level at which the roughness elements absorb the momentum being transferred to the surface. R92 used this definition to derive d. That is, if d_R is the centroid of the form drag on the roughness elements and if d_S is the centroid at which the skin friction acts

$$d\tau = d_R\tau_R + d_S\tau_S = d_R\tau_R \qquad (42)$$

because $d_S = 0$ by definition. Thus

$$d = d_R(\tau_R / \tau). \qquad (43)$$

Notice, from eq 19, 20 and 23

$$\frac{\tau_R}{\tau} = \frac{\lambda(\Phi)\hat{C}_R(\Phi)}{C_{Sh}+\lambda(\Phi)\hat{C}_R(\Phi)}. \qquad (44)$$

R92 then related d_R to h. Following his arguments but applying them to the specific geometry of my model, I get

$$d_R = h - c_d C_{Dh}^{-1/2}\left[A(\Phi)/\lambda(\Phi)\right]^{1/2} \qquad (45)$$

in which c_d is a constant that R92 took to be 0.6. Inserting eq 5 in this and combining it with eq 43 yields

$$d = h(\tau_R / \tau)\left[1 - c_d' C_{Dh}^{-1/2}(mn/2\gamma)^{1/2}\right]. \qquad (46)$$

Thus, it is easy to find τ_R/τ from eq 44; and once my model yields C_{Dh}, it is simple to compute d. Using this value in eq 41 finally gives the quantity we seek, C_{DN10}.

I pointed out in the previous section that we need to convert C_{S10} to C_{Sh} before we can begin computations. Equation 41 also makes this conversion. Unfortunately, we need C_{Sh} before we have obtained d. I could handle this problem by iterating the entire set of equations on d. But, as I will show in the next section, $d/h \approx 0.3$, a result also consistent with eq 46. At this step in the computations, this simple approximation is reasonable—especially in light of uncertainties in the other model parameters—because C_{DN10} is not very sensitive to C_{S10} for the range of values that this parameter can realistically assume.

RESULTS

I have not yet discussed the value of γ, the fractional coverage of sastrugi-like roughness elements. Vladimir Churun* tried to quantify the roughness of the ISW floe using the radar on the *Akademik Fedorov* at the time the station was deployed. His survey suggested that hummock coverage varied over the floe from 10 to 30%. While hummock coverage is not the same as sastrugi coverage, my personal experience on ISW suggests that 10–30% sastrugi coverage is also about right. Notice, because of the geometry of the sastrugi that I am modeling (Fig. 3), the tightest possible packing of roughness elements will yield a γ value of only 0.5. Thus, my first guess,

---

* Personal communication (Arctic and Antarctic Research Institute, St. Petersburg, Russia).

$\gamma = 0.15$, represents a conservative but not insignificantly small sastrugi coverage.

Figure 4 shows two sets of predictions for C_{DN10} as a function of Φ based on the model developed in the preceding section. Figure 4a shows computations of C_{DN10} for $\gamma = 0.15$ and for sastrugi heights of 5, 10 and 20 cm, typical heights represented in our snow-surface roughness surveys (e.g., Fig. 2). The 10-cm case fits our observations quite well. Here, C_{DN10} is $1.43–1.45 \times 10^{-3}$ when the flow is head-on or within $\pm 12°$ of head-on (that is, when $\Phi \lesssim \beta$). These values agree well with the nominal minimum value for C_{DN10} of 1.5×10^{-3} that we reported in AC95.

When Φ gets larger than $11.3°$ (see eq 3), the wind can see the side ridge of the obstacle. In effect, it sees a larger silhouette area and a higher value of C_R; C_{DN10} must thus increase. Figure 4 shows that if the wind rotates just $20°$ from head-on, C_{DN10} will increase by 15–24%, in good agreement with our observations in AC95.

As Φ increases and the wind thus has an increasing component perpendicular to the axis of the sastrugi, C_{DN10} continues increasing. C_{DN10} has its maximum at $\Phi = 101.3°$, where it is 2.73×10^{-3} for the $\gamma = 0.15$ and $h = 10$ cm case. Again, m and n set the location for this maximum; this is where $A(\Phi)$ has its maximum. The C_{DN10} value there is in fair agreement with the maximum value that we observed on ISW, 2.54×10^{-3} (AC95).

As Φ increases toward $180°$, the model is entirely speculative, since we have few data with which to compare such a reversal in the wind and because C_{R3} is the least certain of the form drag coefficients. For now, the decrease as Φ approaches $180°$ seems reasonable because the silhouette area is decreasing rapidly. But the absolute values for C_{DN10} in this region are certainly open to debate.

In Figure 4a, the calculations with h values of 5 and 20 cm are less realistic than for $h = 10$ cm. For $h = 5$ cm, the maximum C_{DN10} value calculated is 8% less than our observed maximum; for $h = 20$ cm, the calculated maximum is 27% higher than what we observed. For all three heights, however,

a. $\gamma = 0.15$ (the sastrugi cover 15% of the surface) and $h = 5, 10,$ and 20 cm.

b. $h = 10$ cm and $\gamma = 0.10, 0.15, 0.20,$ or 0.25. Notice, the $\gamma = 0.15$ line is the same as in Figure 4a
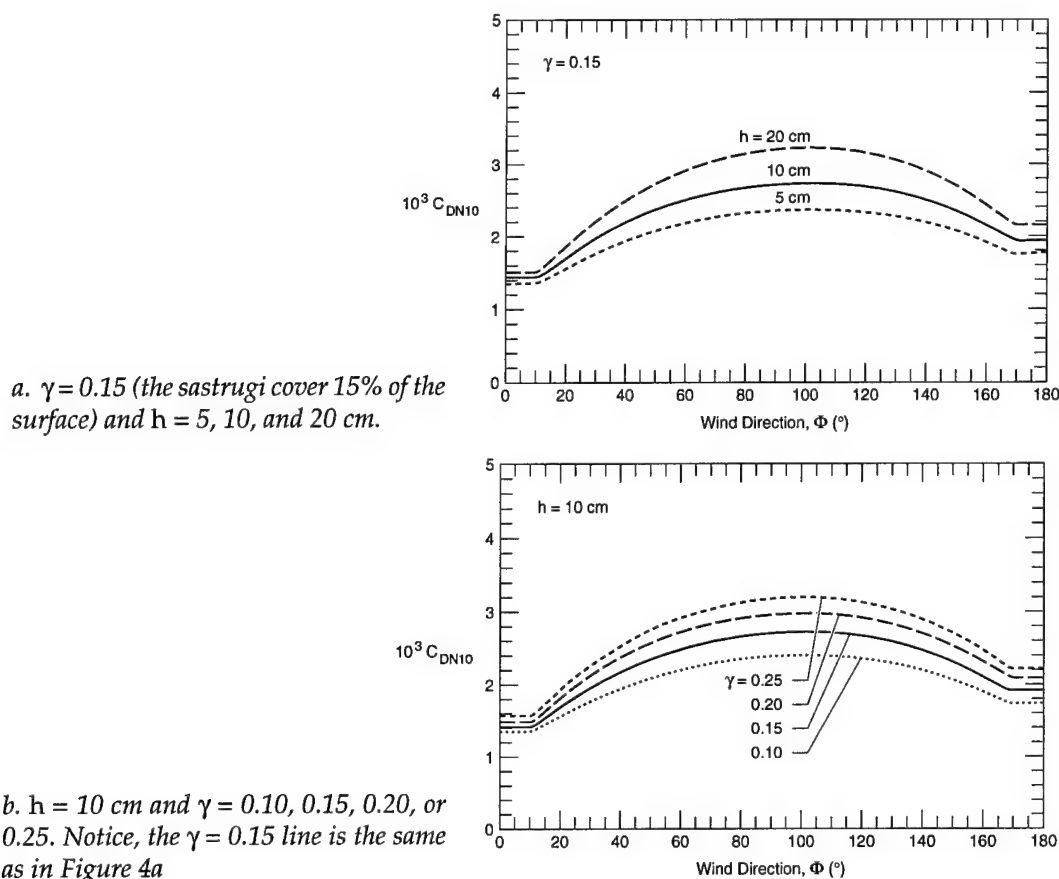
Figure 4. Model calculation of C_{DN10} as a function of the wind orientation (Φ) with respect to the dominant axis of the sastrugi. Model parameters are $m = 4$, $n = 10$, $C_{S10} = 1.10 \times 10^{-3}$, $C_{R1} = 0.10$, $C_{R2} = 0.30$, $C_{R3} = 0.30$, $c = 0.25$, $c_w = 4$ and $c_d = 0.6$.

8

C_{DN10} values for head-on flow are in a reasonable range, $1.36-1.51 \times 10^{-3}$.

Figure 4b investigates the sensitivity of the model to γ when $h = 10$ cm. For this value of h, $\gamma = 0.10$ yields C_{DN10} values for head-on flow of 1.36×10^{-3}. Although we did measure four C_{DN10} values in this range, the more likely lower limit is about 1.5×10^{-3}. Also, as Φ increases, the predicted C_{DN10} values reach a maximum that is 6% below our observed maximum. When γ is 0.20 and 0.25, the predicted head-on values for C_{DN10} are roughly correct, $1.50-1.55 \times 10^{-3}$. But for these γ values, the maximum predicted values are, respectively, 17 and 26% above our observed maximum. Notice, $\gamma = 0.25$ means that the sastrugi cover half the area that they would if they were packed as tightly as possible. This value is, therefore, probably an unrealistically large sastrugi coverage for ISW.

For the $\gamma = 0.15$ and $h = 10$ cm case—the one that fits the data best—I also ran the model with $C_{S10} = 1.00 \times 10^{-3}$ (not shown), roughly the smallest value compatible with the surveys I cited earlier. Resulting predictions for C_{DN10} were 4–6% lower for $0° \leq \Phi \leq 20°$ and for $160° \leq \Phi \leq 180°$ than for calculations based on $C_{S10} = 1.10 \times 10^{-3}$. For $30° \leq \Phi \leq 160°$, the differences were only 2–3%. Consequently, the choice of C_{S10} does not have a big effect on the results, as long as the value is a reasonable one. Secondly, my handling of the displacement height in converting from C_{S10} to C_{Sh} is appropriate, given this weak sensitivity to C_{S10}.

Figure 5 shows some examples of how stress is partitioned between form drag and skin friction. I plot τ_R/τ; clearly, $\tau_S/\tau = 1 - \tau_R/\tau$. In the figure, the ($\gamma = 0.10$, $h = 10$ cm) and the ($\gamma = 0.20$, $h = 20$ cm) lines, respectively, show the minimum and maximum values of τ_R/τ that I obtained for the range of model parameters considered. My computations suggest that, even for a very rough surface, $\gamma = 0.20$ and $h = 20$ cm, skin friction produces more than half of the total stress when the flow is approximately head-on. In other words, the streamlined shape of the sastrugi is quite effective at reducing form drag. When the flow is at right angles to the sastrugi, however, form drag dominates the total stress because the wind has so much more surface to push against. This dominance of form drag for such wind orientations explains why the drifts erode so quickly (AC95).

Equation 46 yields the displacement height; Figure 6 shows several computations of d/h. For

Figure 5. Stress partitioning, τ_R/τ, versus the mean wind direction with respect to the dominant axis of the sastrugi. Realize that $\tau_S/\tau = 1-\tau_R/\tau$. Here, γ is the fractional sastrugi coverage, and h is the sastrugi height in centimeters.
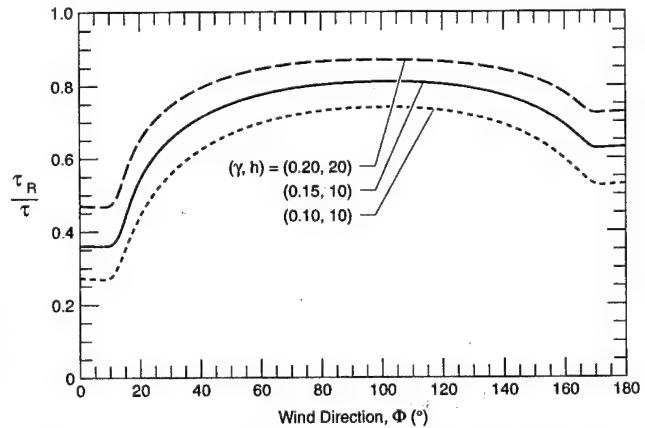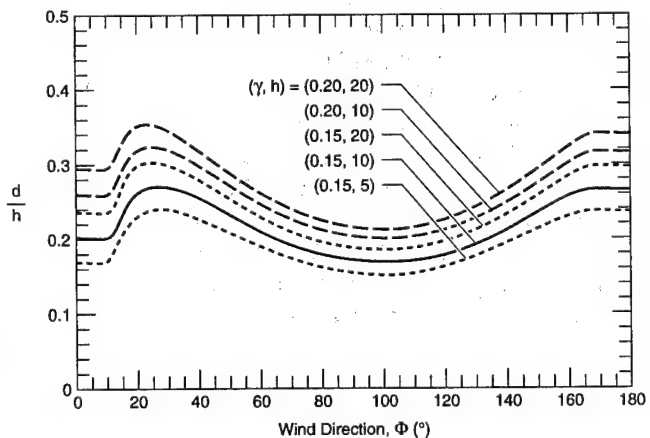

Figure 6. Computed displacement height d scaled by sastrugi height h versus the direction of the mean wind with respect to the sastrugi. Here, γ is the fractional sastrugi coverage, and h is in centimeters.

densely packed roughness elements, such as crops, trees or other vegetation, d/h is typically reported to be about 0.7 (Stanhill 1969, Thom 1971, Fazu and Schwerdtfeger 1989). For the more widely spaced sastrugi that I am considering, however, d/h is 0.15–0.35. This is also roughly what R92 (his Figure 5) computed for λ values in the range relevant to this problem, 0.01–0.06.

These plots justify my use of $d/h = 0.3$ when I had to convert C_{S10} to C_{Sh} in the section on *Partitioning the Stress*. They also show that, for sastrugi typically 10 cm high, d is usually less than 3 cm. We were thus safe to ignore d in analyzing our wind speed profiles in AC95. For the lowest profiling level used in AC95, 0.5 m, including a displacement height of 3 cm in a computation based on eq 29 would yield a u_* value roughly 1% larger than a computation with $d = 0$. For the higher levels, the difference would be even less. Since the nominal uncertainty in our wind speed measurements was ±5 cm/s, this small bias in our computations is negligible.

Figure 6 shows that d has some interesting structure—it is not a constant for all wind directions. Equation 46 explains this behavior: d/h responds mainly to two variables, τ_R/τ and C_{Dh}; d/h increases linearly with τ_R/τ but decreases linearly with $C_{Dh}^{1/2}$. The peak in d/h near 20–30° corresponds to the rapid increase in τ_R/τ in this range (Fig. 5), while the broad minimum centered near 100° is where C_{Dh} has its maximum (Fig. 4). Another curious feature in Figure 6 is that the d values in this broad minimum are usually less than the values for head-on flow. Clearly, d does not change in concert with z_0 or C_{Dh}—parameters that quantify the aerodynamic roughness of the surface. This is an important conclusion because others have claimed that d is a linear function of z_0 (e.g., Brutsaert 1982, p. 113; Sugita and Brutsaert 1990).

In summary, the *Raupach's Model Adapted to Drifting Snow* section explains that my adaptation of R92's model has 11 adjustable parameters: h, m, n, γ, C_{S10}, C_{R1}, C_{R2}, C_{R3}, c, c_w and c_d. With reasonable choices for these and with little fine-tuning, I have demonstrated that that model fits our ISW observations quite well. I do not mean to imply here, however, that the model is infallibly accurate—only that it seems to capture the essential physics of how wind transfers momentum to snow-covered sea ice.

DISCUSSION

Primary roughness elements

The obvious (and, perhaps, surprising) conclusion from the calculations described in the last section is that roughness elements with heights of only 10 cm can have a dominant effect on C_{DN10}. This is essentially the same conclusion that Jackson and Carroll (1978) reached. Arya's (1973, 1975) model, in contrast, predicted that pressure ridges 1 to 4 m high accounted for most of the form drag that determined the large-scale roughness and drag coefficient over Arctic sea ice.

My calculations provide a theoretical basis for the empirical result that Banke et al. (1976, 1980) obtained, eq 1. Their roughness parameter ξ reflects the small-scale roughness; they reported ξ values of 3–13 cm, where ξ came from integrating the roughness spectrum over all wavelengths shorter than 13 m (also see Andreas et al. 1993). Such wavelengths are far smaller than either Arctic or Antarctic ridge spacings (Lytle and Ackley 1991). Thus, eq 1 and my calculations point to the same conclusion: Pressure ridges are relatively unimportant in setting the local drag coefficient; C_{DN10} responds primarily to sastrugi-size roughness elements. Pressure ridges, however, will probably be important in establishing an areally averaged or effective roughness length, Z_0. Fiedler and Panofsky (1972), Arya (1975), Overland (1985), and Claussen (1991), among others, have offered some thoughts on inferring Z_0 from z_0. But pursuing that connection is beyond my scope here.

Parameterizing the drag coefficient

These model results and the behavior of C_{DN10} over snow-covered sea ice that we documented in AC95 suggest what might be necessary in a scheme for parameterizing C_{DN10}. The snow surface is not in general isotropic, especially during, or for some time after, high wind events. The wind builds sastrugi and therefore streamlines the surface in the mean wind direction. Figure 4 shows how C_{DN10} behaves for various wind directions once the surface has been streamlined.

Thus, the key is to estimate the dominant direction of the sastrugi without the benefit of in situ observations. Maybe in the future, satellites will provide real-time information on ice-surface roughness, including any preferential alignment of the roughness elements. But for now, all we can

do is estimate the orientation of roughness elements by tracking the history of surface winds that have been inferred from analyzed geostrophic winds. According to AC95, if the surface wind blows at 8 m/s or higher with constant direction, it will build sastrugi parallel to it and, thus, streamline the surface. If such conditions persist for 12 hours, C_{DN10} will fall from its initial value to about 1.5×10^{-3} and will remain here as long as the wind remains aligned with the sastrugi.

If subsequent surface winds fall below 6 m/s, Figure 4 shows how C_{DN10} will vary as the wind turns with respect to the axis of the sastrugi.

The difficult part of the parameterization will be treating directionally variable winds of 6–8 m/s, or higher. These are strong enough to begin reworking the surface—eroding the snowdrifts present—but, because of their variability, will not necessarily build new drifts and thereby streamline the surface in another direction. Neither the data in AC95 nor the model developed here provides a clear suggestion on how to evaluate C_{DN10} for such winds.

In summary, except for the complication just mentioned, it seems possible to now estimate C_{DN10} over snow-covered sea ice by tracking the history of the surface wind computed from analyzed pressure fields. I have described the algorithm in words; coding and testing it is the next step.

CONCLUSIONS

I have adapted R92's model for the form drag on a field of interacting roughness elements and applied it to rudimentary sastrugi-like snowdrifts. The key step was treating the complex geometry of the sastrugi. In the absence of laboratory values for the form drag on the various faces of the sastrugi, I assumed that the form drag reflects additive contributions from the various faces of the individual sastrugi (see eq 13).

The resulting model does quite well in reproducing the values of C_{DN10} that we observed in AC95. For sastrugi of height 10 cm and with an areal coverage of 15%, the model predicts that $C_{DN10} = 1.43 \times 10^{-3}$ when Φ is less than 12°. In AC95, the nominal head-on value of C_{DN10} that we observed was 1.5×10^{-3}. In the model, as Φ gets larger than 12°, C_{DN10} increases rapidly. In this example, C_{DN10} increases by 17% as Φ turns from 12 to 20°. As Φ continues increasing, C_{DN10} eventually reaches a maximum of 2.73×10^{-3} at

$\Phi = 101.3°$. This increase with Φ also mirrors the directional sensitivity we reported in AC95, though the predicted maximum is about 7% higher than our measured maximum for C_{DN10}, 2.54×10^{-3}.

The upshot of this modeling is that the small, 10-cm-high roughness elements associated with drifting snow—rather than pressure ridges or other mesoscale features—determine the local drag coefficient over snow-covered sea ice. Though some have stated this conclusion explicitly (e.g., Joffre 1982) or implicitly (e.g., Banke et al. 1976, 1980), my model is the first to provide a theoretical foundation for it.

These model predictions and the observations in AC95 suggest how we should attempt to parameterize C_{DN10} in terms of what we can measure. Because C_{DN10} depends crucially on how the mean wind is oriented with respect to the sastrugi, the key is predicting sastrugi orientation. Our observations showed that this orientation depends on the history of the surface wind. By inferring surface winds from analyzed fields of the geostrophic wind, we should be able to deduce this orientation. The event to look for is a directionally constant surface wind of at least 8 m/s that persists for 12 hours. At the end of such an event, C_{DN10} will be roughly 1.5×10^{-3}. Figure 4 then shows how to estimate C_{DN10} when the wind direction subsequently changes.

LITERATURE CITED

Allen, J.R.L. (1965) Scour marks in snow. *Journal of Sedimentary Petrology*, **35**: 331–338.

Andreas, E.L and K.J. Claffey (1995) Air–ice drag coefficients in the western Weddell Sea: 1. Values deduced from profile measurements. *Journal of Geophysical Research*, **100**: 4821–4831.

Andreas, E.L, M.A. Lange, S.F. Ackley and P. Wadhams (1993) Roughness of Weddell Sea ice and estimates of the air–ice drag coefficient. *Journal of Geophysical Research*, **98**: 12,439–12,452.

Arie, M. and H. Rouse (1956) Experiments on two-dimensional flow over a normal wall. *Journal of Fluid Mechanics*, **1**: 129–141.

Arya, S.P.S. (1973) Contribution of form drag on pressure ridges to the air stress on Arctic ice. *Journal of Geophysical Research*, **78**: 7092–7099.

Arya, S.P.S. (1975) A drag partition theory for determining the large-scale roughness parameter and wind stress on the Arctic pack ice. *Journal of Geophysical Research*, **80**: 3447–3454.

Banke, E.G. and S.D. Smith (1973) Wind stress on Arctic sea ice. *Journal of Geophysical Research*, **78**: 7871–7883.

Banke, E.G., S.D. Smith and R.J. Anderson (1976) Recent measurements of wind stress on Arctic sea ice. *Journal of the Fisheries Research Board of Canada*, **33**: 2307–2317.

Banke, E.G., S.D. Smith and R.J. Anderson (1980) Drag coefficients at AIDJEX from sonic anemometer measurements. In *Sea Ice Processes and Models* (R.S. Pritchard, Ed.). Seattle: University of Washington Press, p. 430–442.

Brutsaert, W.H. (1982) *Evaporation into the Atmosphere: Theory, History and Applications*. Dordrecht: D. Reidel.

Claussen, M. (1991) Estimation of areally-averaged surface fluxes. *Boundary-Layer Meteorology*, **54**: 387–410.

Fazu, C. and P. Schwerdtfeger (1989) Flux-gradient relationships for momentum and heat over a rough natural surface. *Quarterly Journal of the Royal Meteorological Society*, **115**: 335–352.

Fiedler, F. and H.A. Panofsky (1972) The geostrophic drag coefficient and the 'effective' roughness length. *Quarterly Journal of the Royal Meteorological Society*, **98**: 213–220.

Finney, E.A. (1939) Snow drift control by highway design. Engineering Experiment Station, Michigan State College, East Lansing, Bulletin 86.

Jackson, B.S. and J.J. Carroll (1978) Aerodynamic roughness as a function of wind direction over asymmetric surface elements. *Boundary-Layer Meteorology*, **14**: 323–330.

Joffre, S.M. (1982) Momentum and heat transfers in the surface layer over a frozen sea. *Boundary-Layer Meteorology*, **24**: 211–229.

Kondo, J. and H. Yamazawa (1986) Bulk transfer coefficient over a snow surface. *Boundary-Layer Meteorology*, **34**: 123–135.

Kutzbach, J.E. (1961) Investigation of the modification of wind profiles by artificially controlled surface roughness. In Annual Report 1961, Department of Meteorology, University of Wisconsin, Madison, p. 71–113.

Lettau, H. (1969) Note on aerodynamic roughness-parameter estimation on the basis of roughness-element description. *Journal of Applied Meteorology*, **8**: 828–832.

Lytle, V.I. and S.F. Ackley (1991) Sea ice ridging in the eastern Weddell Sea. *Journal of Geophysical Research*, **96**: 18,411–18,416.

Mellor, M. (1965) Blowing snow. USA Cold Regions Research and Engineering Laboratory, Cold Regions Science and Engineering Monograph, Part III, Section A3c.

Overland, J.E. (1985) Atmospheric boundary layer structure and drag coefficients over sea ice. *Journal of Geophysical Research*, **90**: 9029–9049.

Owen, P.R. (1964) Saltation of uniform grains in air. *Journal of Fluid Mechanics*, **20**: 225–242.

Plate, E.J. (1971) *Aerodynamic Characteristics of Atmospheric Boundary Layers*. Oak Ridge, Tennessee: U.S. Atomic Energy Commission.

Radok, U. (1968) Deposition and erosion of snow by the wind. USA Cold Regions Research and Engineering Laboratory, Research Report 230.

Raupach, M.R. (1992) Drag and drag partition on rough surfaces. *Boundary-Layer Meteorology*, **60**: 375–395.

Raupach, M.R., D.A. Gillette and J.F. Leys (1993) The effect of roughness elements on wind erosion threshold. *Journal of Geophysical Research*, **98**: 3023–3029.

Stanhill, G. (1969) A simple instrument for the field measurement of turbulent diffusion flux. *Journal of Applied Meteorology*, **8**: 509–513.

Sugita, M. and W. Brutsaert (1990) Wind velocity measurements in the neutral boundary layer above hilly prairie. *Journal of Geophysical Research*, **95**: 7617–7624.

Taylor, P.A. (1988) Turbulent wakes in the atmospheric boundary layer. In *Flow and Transport in the Natural Environment: Advances and Applications* (W.L. Steffen and O.T. Denmead, Eds.). Berlin: Springer-Verlag, p. 270–292.

Thom, A.S. (1971) Momentum absorption by vegetation. *Quarterly Journal of the Royal Meteorological Society*, **97**: 414–428.

REPORT DOCUMENTATION PAGE

Form Approved
OMB No. 0704-0188

1. AGENCY USE ONLY (Leave blank)	2. REPORT DATE July 1995	3. REPORT TYPE AND DATES COVERED

4. TITLE AND SUBTITLE

A Physically Based Model of the Form Drag
Associated with Sastrugi

5. FUNDING NUMBERS

OPP-90-24544
OPP-93-12642
PR: 4A161102AT24

6. AUTHORS

Edgar L Andreas

7. PERFORMING ORGANIZATION NAME(S) AND ADDRESS(ES)

U.S. Army Cold Regions Research and Engineering Laboratory
72 Lyme Road
Hanover, New Hampshire 03755-1290

8. PERFORMING ORGANIZATION REPORT NUMBER

CRREL Report 95-16

9. SPONSORING/MONITORING AGENCY NAME(S) AND ADDRESS(ES)

Office of Polar Programs
National Science Foundation
Arlington, Virginia

Office of the Chief of Engineers
Washington, DC 20314-1000

10. SPONSORING/MONITORING AGENCY REPORT NUMBER

11. SUPPLEMENTARY NOTES

12a. DISTRIBUTION/AVAILABILITY STATEMENT

Approved for public release; distribution is unlimited.

Available from NTIS, Springfield, Virginia 22161.

12b. DISTRIBUTION CODE

13. ABSTRACT *(Maximum 200 words)*

On Ice Station Weddell, some characteristics of the neutral-stability air–ice drag coefficient at a reference height of 10 m (C_{DN10}) were observed that had not been documented before. The main finding was that wind-driven snow continually alters the sea ice surface; the resulting snowdrifts determine how large C_{DN10} is. In particular, this report describes three observations and attempts to explain them: 1) C_{DN10} is near 1.5×10^{-3} when the wind is well aligned with the drifted snow; 2) C_{DN10} is near 2.5×10^{-3} when the wind makes a large angle with the dominant orientation of the snowdrifts; 3) C_{DN10} can increase by 20% if, after being well aligned with the drift patterns, the mean wind direction shifts by as little as 20°. To investigate this behavior of C_{DN10}, this report adapts a model developed by Raupach that partitions the total surface stress into contributions from form drag and skin friction. With reasonable choices for free model parameters and with little fine-tuning, this physically based model can reproduce the three main observations. In other words, the model seems to include the basic physics of air–ice momentum exchange. This modeling implies that 10-cm-high sastrugi-like roughness elements, rather than pressure ridges, sustain most of the form drag over compact sea ice in the western Weddell Sea. Lastly, the report speculates on what the observations and this model say about how to parameterize C_{DN10} over snow-covered sea ice.

14. SUBJECT TERMS

Air–sea–ice interaction
Drag coefficient
Drifting snow
Form drag
Snow drifts
Weddell Sea

15. NUMBER OF PAGES
14

16. PRICE CODE

17. SECURITY CLASSIFICATION OF REPORT	18. SECURITY CLASSIFICATION OF THIS PAGE	19. SECURITY CLASSIFICATION OF ABSTRACT	20. LIMITATION OF ABSTRACT
UNCLASSIFIED	UNCLASSIFIED	UNCLASSIFIED	UL

NSN 7540-01-280-5500

Standard Form 298 (Rev. 2-89)
Prescribed by ANSI Std. Z39-18
298-102